Morphology and Fracture Properties of Pure and Reinforced Aluminum-Epoxy Adhesive Joints

JOVAN MIJOVIĆ, *Polytechnic Institute of New York, Department of Chemical Engineering, 333 Jay Street, Brooklyn, New York 11201*

Synopsis

Several types of nonreinforced and reinforced epoxy-aluminum adhesive joints were prepared and investigated. High modulus carbon fibers and hollow glass microspheres were used as reinforcement. The amount of curing agent, postcure time, adhesive thickness, and type and amount of reinforcement were varied throughout this study, and their effect on fracture energy was determined. Unstable crack propagation through the adhesive layer was observed. Nodular morphology typified all fracture surfaces of nonreinforced adhesive joints, indicating the existence of an inhomogeneous thermosetting network. Electron microscopic evidence was obtained for plastic flow in crack initiation and crack arrest regions. The nature of this plastic flow was discussed in terms of changes in the resin morphology.

INTRODUCTION

In spite of the extensive application of thermosetting polymers as adhesives, little is known about correlations between their morphology and ultimate mechanical properties. An ever-increasing use of thermosets as adhesives dictates that the design criteria for these materials be based upon the reliability against brittle fracture. Methods of linear elastic fracture mechanics[1-3] (LEFM) analysis have been employed extensively to calculate the fracture energy (strain energy release rate) of adhesive joints. The critical value of strain energy release rate, at given loading rate and environmental conditions, represents a geometric independent material property and as such is suitable for specifying the ultimate mechanical properties and requirements of structural materials. The strain energy release rate can be thought of as the energy required to extend a preexisting crack an infinitesimal unit of area. A critical value of the strain energy release rate[2] at which the crack extends in mode I is designated $\mathcal{G}_{Ic}$. An expression for $\mathcal{G}_{Ic}$ is given by

$$\mathcal{G}_{Ic} = \frac{dU}{dA} = \frac{dU}{Bda} = \frac{P_c^2}{2B}\left(\frac{\partial C}{\partial a}\right)_P \tag{1}$$

where $\mathcal{G}_{Ic}$ (J/m^2) is the critical strain energy release rate, P_c (kg$_f$) is the critical load, B (cm) is the specimen width, and $(\partial C/\partial a)_P$ is the change of compliance with crack length at constant load. Uniform double cantilever beam (UDCB) arrangements employed in earlier studies[4,5] represented an elaboration of Obreimoff's experiment[6] on the cleavage of mica, carried out in 1930.

In the mid-sixties, a system was designed[7,8] with a constant compliance change with crack length (dC/da = const) by varying the height of the specimen along the crack propagation path. Contoured specimens of this type are referred to as tapered double-cantilever beam (TDCB) specimens. Experimentally, the

Journal of Applied Polymer Science, Vol. 25, 1179–1193 (1980)

0021-8995/80/0025-1179$01.50

critical strain energy release rate can be calculated readily as a function of the critical load only.[8]

Fracture energies of various epoxy adhesive systems, as obtained from the cleavage tests of TDCB specimens, have been reported by several workers.[7,9–18]

On the other hand, the morphology of thermosetting resins has recently become a subject of considerable practical and scientific interest, since many anomalous findings in studies of mechanical properties of thermosets could be rationalized in terms of an inhomogeneous network.[19] It is now generally agreed that the morphology of highly crosslinked thermosets is composed of the more highly crosslinked nodules, ranging in size from 6 nm to 10 μm, surrounded by a less highly crosslinked lower molecular weight matrix. Therefore, attempts were made in this study to describe the nodular morphology of fracture surfaces. Finally, since most crack propagation paths in brittle thermosets are characterized by a certain amount of plastic flow in crack initiation and crack arrest zones, special attention was paid to the morphology of these regions.

EXPERIMENTAL

Chemical Systems

The chemical structure of epoxy resin and curing agent used in this work is presented in Table I. Reinforcing materials are described in Table II. The composition and cure schedule of various epoxy resin formulations are listed in Table III.

Techniques

The exact method of manufacturing the tapered double-cantilever aluminum beams, as well as the specimen dimensions, are given in the ASTM D 3433-75. A phosphoric acid anodize bath represents an addition to the usual cleaning procedure for aluminum beams and gives rise to an improved adhesion between aluminum and various thermosetting adhesives.[20] Priming preserves optimally

TABLE I
Chemical Structure of Epoxy Resin and Curing Agent

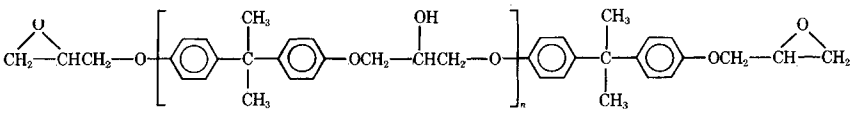

Typical diglycidyl ether of bisphenol-*A* (DGEBA) resin[a]

$$H_2N—CH_2—CH_2—NH—CH_2—CH_2—NH_2$$

Diethylene triamine[b] (DETA) curing agent

[a] Epon 825, Shell's liquid DGEBA resin used in this study, is a purified form of commercially available EPON 826.

[b] DETA was supplied by the Aldrich Chemical Company.

TABLE II
Reinforcing Particles for Adhesive Systems

Reinforcement	Concentration level	Manufacturer	Specifications, comments
Chopped carbon fibers	5 phr[a]	Union Carbide	Made from pitch, high modulus fibers, $E = 45 \times 10^5$ psi.
Sodium borosilicate hollow glass microspheres	10 phr	Emerson and Cuming Inc. Eccospheres IG-101	Particle size ranging from 20 to 200 μm, average (weight basis) particle diameter: 80 μm, average wall thickness (weight basis): 2 μm. Untreated surfaces.

[a] phr denotes parts per hundred parts of resin, by weight.

etched aluminum surfaces and allows the use of beams after an indefinite period of time.

Upon priming, the bonding surfaces were ready for the application of the adhesive. Resin, curing agent, and reinforcement were thoroughly mixed for 5 min

TABLE III
Various Adhesive Formulations Studied

Formulation or cure schedule No.	Composition	Variable	Adherend	Cure schedule
1	Epon 825 + 11 phr DETA	Postcure time	Al	Components mixed at RT,[a] applied onto bonding surfaces after 1 hr and 25 min, surfaces brought together after additional 30 min. 1 hr at RT under pressure (6 psi) + 23 hr at 72°F and 45% RH[b] + postcure 120°C.
2	Epon 825 + 11 phr DETA	Adhesive thickness	Al	Components mixed at RT, immediately poured into casting dam. 2 hr at RT + 23 hr at 120°C.
3	Epon 825 + 25 phr DETA + 5 phr C fibers	Postcure time	Al	Components mixed at RT, applied onto bonding surfaces after 1 hr, brought together after additional 20 min. 1 hr at 85°F under pressure (6 psi) + postcure at 120°C.
4	Epon 825 + 8 phr DETA + 5 phr C fibers	Postcure time	Al	Components mixed at 60°C, applied onto bonding surfaces after 15 min, surfaces brought together immediately. 1 hr at 85°F under pressure (6 psi) + postcure at 120°C.
5	Epon 825 + 11 phr DETA + 10 phr glass spheres	Adhesive thickness	Al	Same as formulation 2

[a] Room temperature (RT).
[b] Relative humidity (RH).

and further cure was conducted, as outlined in Table III. The actual application of the adhesive on the beams is described elsewhere.[2] All samples were kept at 72°F and 45% relative humidity for at least 24 hr prior to testing. An Ametek-Riehle Testing Equipment system was used for the fracture energy measurements. All tests were performed at a crosshead speed of 0.2 in./min.

One-stage and two-stage carbon–platinum (C–Pt) replicas of various fracture surfaces were made and studied by transmission electron microscopy (TEM). Also, parts of fracture surfaces were gold shadowed and studied by scanning electron microscopy (SEM). The sample preparation methods for TEM and SEM studies are described elsewhere.[21] A Cwikscan 100 scanning electron microscope and a JEOL 100B transmission electron microscope were used to investigate the fracture surfaces.

RESULTS

Fracture Tests

All investigated specimens, nonreinforced and reinforced, exhibited an apparent cohesive [center of bond (CoB)] failure. Also, an unstable crack propagation, characterized by the "saw-toothed" appearance in load-displacement diagrams, was observed in all cases.

Pure Epoxy Adhesives

Figure 1 shows the critical strain energy release rate for crack initiation ($\mathcal{G}_{Ici}$)

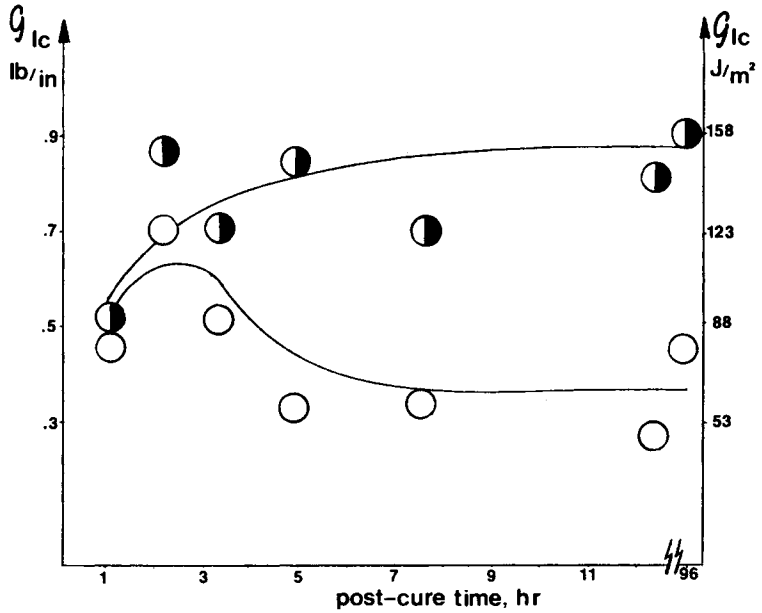

Fig. 1. Critical strain energy release rate as a function of postcure time for an aluminum-epoxy adhesive system subjected to cure schedule 1 (Table III).

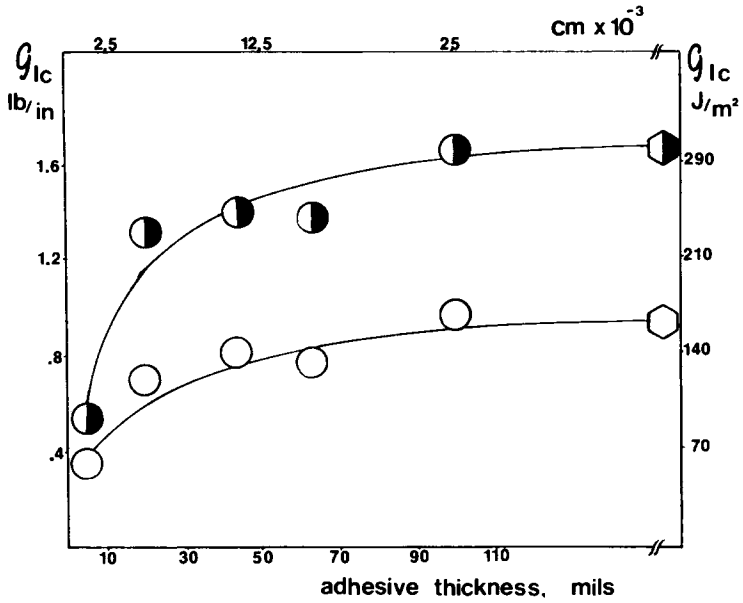

Fig. 2. Critical strain energy release rate as a function of adhesive thickness for an aluminum–epoxy adhesive system subjected to cure schedule 2 (Table III). (◑) $\mathcal{G}_{Ici}$; (○) $\mathcal{G}_{Ica}$; (◑) $\mathcal{G}_{Ici}$ (bulk); (○) $\mathcal{G}_{Ica}$ (bulk).

and arrest ($\mathcal{G}_{Ica}$) as a function of postcure time. A sudden increase in $\mathcal{G}_{Ic}$ was noted at short postcure times. In spite of the certain amount of data scatter, it appears that $\mathcal{G}_{Ici}$ and $\mathcal{G}_{Ica}$ follow similar patterns. Moreover, their difference ($\Delta\mathcal{G}_{Ic} = \mathcal{G}_{Ici} - \mathcal{G}_{Ica}$) increases with postcure time, displaying the same trend observed earlier with the bulk resin.[21]

The effect of varying adhesive thickness on adhesive fracture energy was studied next. Figure 2 indicates a steep increase in both $\mathcal{G}_{Ici}$ and $\mathcal{G}_{Ica}$ up to the adhesive thickness of approximately 400 μm. After that point, only a slight upward trend was noted; the $\mathcal{G}_{Ic}$ value remained essentially constant. $\mathcal{G}_{Ici}$ and $\mathcal{G}_{Ica}$ values at the largest adhesive thickness are the extrapolated values of corresponding (identical composition and cure schedule) bulk specimens.[22] An interesting visual observation was made with thicker specimens in that the crack propagation path had a tendency to migrate between the two adherends, as shown in Figure 3. Nonetheless, the fracture was strictly cohesive in the resin; no interfacial (IF) failure was detected.

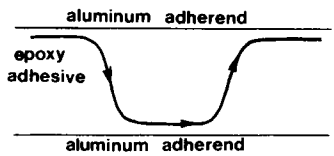

Fig. 3. Schematic presentation of the observed crack propagation path (indicated by arrows) showing sudden jumps across the adhesive layer. Note, however, that at all times cohesive failure in the adhesive takes place.

Carbon Fiber Reinforced Epoxy Adhesives

The results obtained with two different carbon-fiber (C-fiber) reinforced epoxy systems (formulations 3 and 4, Table III) are presented next. The pure epoxy formulation already studied (formulation 1, Table III) was compared to the same system (identical composition and cure) containing additional 5 phr of C-fibers. Interestingly, in order to achieve approximately the same curing rate at room temperature, an excess of 14 phr of curing agent (25 phr DETA total) had to be added to the latter system. A rather swift increase in fracture energy was observed before the asymptotic value was attained at postcure time of approximately 8 hr, as shown in Figure 4. The $\Delta\mathcal{G}_{Ic}$ value again showed a steady rise before reaching the asymptote. It is worth noting, however, that $\Delta\mathcal{G}_{Ic}$, as a function of postcure time, reaches its asymptotic value earlier than the corresponding value of bulk specimens.[21]

Next, the amount of curing agent was reduced and the initial mixing temperature raised to 60°C (formulation 4, Table III). In spite of only 8 phr DETA present in the system, the curing rate was enhanced and the resin had to be applied onto adherend surfaces within 15 min of mixing. Fracture energy values remained relatively constant during the first 6 hr of postcure (with the exception of the value at 2 hr) and then increased steadily, as seen in Figure 5. Note that the last data point taken (19 hr) was still on an ascending line. Consequently, the $\Delta\mathcal{G}_{Ic}$ value would probably have a tendency to increase beyond the last data point. This behavior is different from the C-fiber reinforced system previously described and is rather similar to the bulk system.

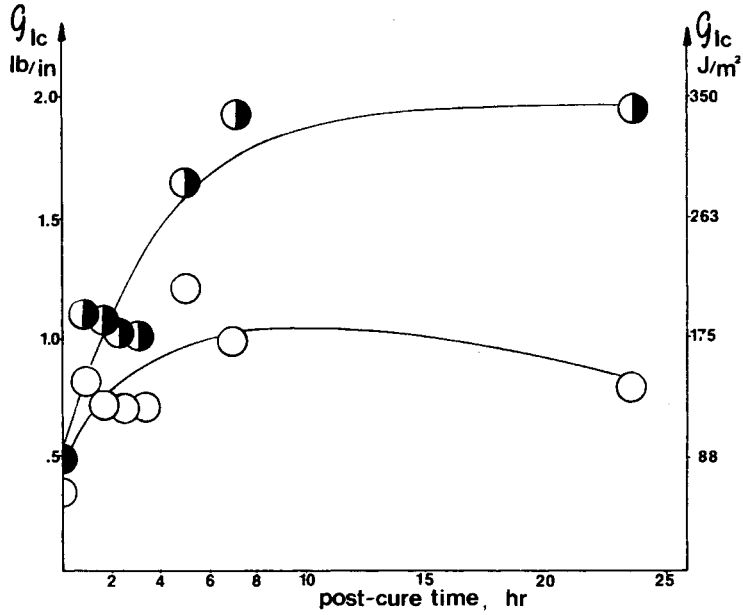

Fig. 4. Critical strain energy release rate as a function of postcure time for an aluminum–carbon fiber reinforced epoxy adhesive system subjected to cure schedule 3 (Table III). Symbols as in Figure 1.

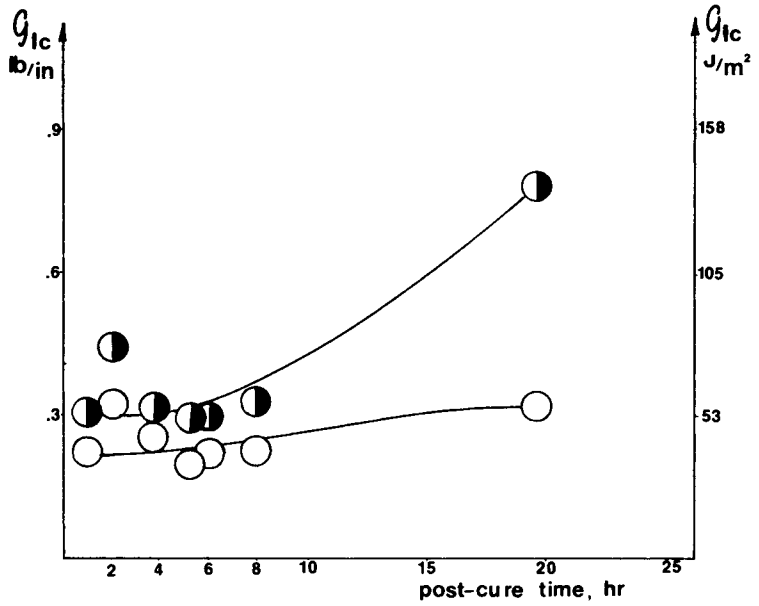

Fig. 5. Critical strain energy release rate as a function of postcure time for an aluminum–carbon fiber reinforced epoxy adhesive system subjected to cure schedule 4 (Table III). Symbols as in Figure 1.

Glass Microsphere Reinforced Epoxy Adhesives

A slight upward trend in $\mathcal{G}_{Ic}$ with increased adhesive thickness was noted, as shown in Figure 6. No data points were taken at adhesive thicknesses of less than 380 μm, since the size of the largest microspheres was approximately 200 μm. Crack propagated in an unstable manner, following the path depicted in Figure 3. Only a slight increase in $\Delta\mathcal{G}_{Ic}$ with increased adhesive thickness was seen. Interestingly, the obtained values of $\mathcal{G}_{Ici}$ and $\mathcal{G}_{Ica}$ lie below the corresponding values for pure (nonreinforced) epoxy adhesive.

Microscopy

Nodular Morphology of Fracture Surfaces of Pure Epoxy Adhesives

Transmission electron micrographs (TEM) of the regions in which a fast crack propagation through the adhesive took place showed clearly the absence of any appreciable difference between fracture morphologies of pure epoxy adhesives and bulk epoxy resins.[19] A distinct nodular morphology characterized all surfaces. Fracture proceeded around nodules whose size and distribution did not change with either postcure time (1–24 hr), replica location, or adhesive thickness. The size of nodules on all fracture surfaces corresponded closely to that of bulk specimens of identical curing agent concentration.[19] A TEM micrograph of a fracture surface of pure epoxy adhesive is shown in Figure 7.

A typical SEM micrograph of crack arrest and crack initiation regions, characterized by an apparent plastic flow, is shown in Figure 8. Before arresting, a crack propagates in what appears to be an elastic manner through the region typified by nodular morphology. No significant plastic flow was detected in that

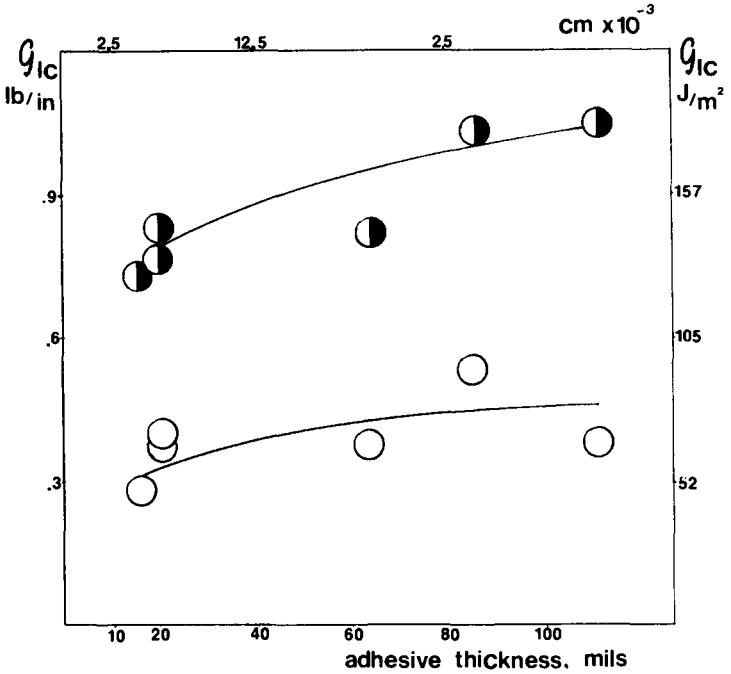

Fig. 6. Critical strain energy release rate as a function of adhesive thickness for an aluminum–glass microsphere reinforced epoxy adhesive system subjected to cure schedule 5 (Table III). Symbols as in Figure 1.

area because of the high crack speed; however, as the crack speed changes, an increased inelastic deformation causes the local crack extension force to drop below the critical value of strain energy release rate, at which point the crack arrests. When the critical value of strain energy release rate is reached again, crack initiation occurs at many points along the width of the beam. The re-initiation starts slowly with cracks often re-initiating in a plane different from that in which they had arrested. The initiation marks (steps or ridges) created by plastic flow are visible to the naked eye. Nonetheless, the plastic deformation region extends only over a relatively small length of approximately several hundred microns. Beyond that point the critical value of strain energy release rate is reduced and fast crack propagation, characterized by a mirror-smooth appearance to the naked eye, takes place.

From a thorough microscopic investigation of upper and lower beams, it appears that tearing ridges on the upper beam correspond to ridges on the lower beam. Similar observation has been reported by Patrick[23] who maintains that the upper beam is a mirror-image rather than a male-female fit of the lower beam at the arrest site.

A more detailed image of the nature of plastic flow was obtained by the TEM technique because of its higher resolution. When enough energy for crack initiation is supplied to the system, a steplike fracture occurs along the rows of initiation sites, as seen in Figure 9. Energy dissipated in this flow is included in the measured $\mathcal{G}_{Ic}$ value.

The overall appearance of an arrest zone was characterized by numerous steps, smaller than those of an initiation zone as seen clearly in Figures 8 and 9.

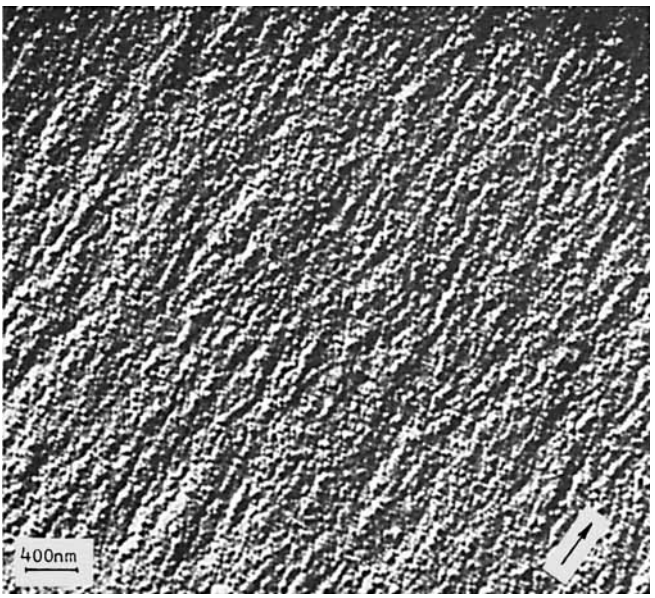

Fig. 7. Transmission electron micrograph of a one-stage C–Pt replica of fracture surface of pure epoxy adhesive subjected to cure schedule 1 (Table III). Magnification 25,000×. Note characteristic nodular morphology.

Finally, careful examination of areas near the steps along which the crack propagation occurs indicate that no significant deformation of nodules takes place, not even in the proximity of the sharp edge of a step. Similar observation in bulk resins is illustrated elsewhere.[19]

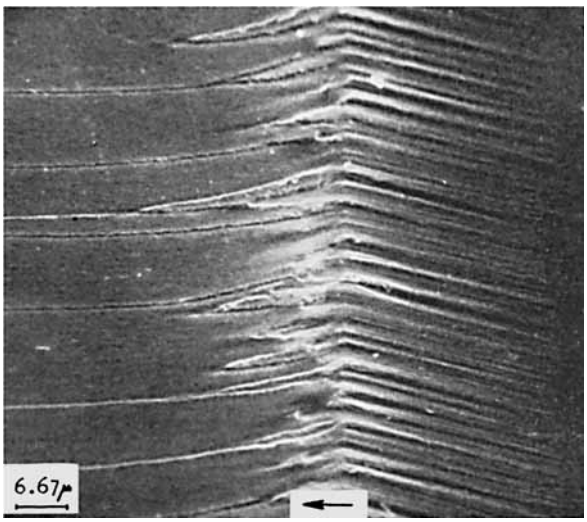

Fig. 8. Scanning electron micrograph of a fracture surface of pure epoxy adhesive subjected to cure schedule 1 (Table III). Magnification 1500×. Note crack initiation and crack arrest regions. The arrow on this and all subsequent micrographs indicates crack propagation direction.

Fig. 9. Transmission electron micrograph of a one-stage C–Pt replica of initiation and arrest regions on a fracture surface of pure epoxy adhesive subjected to cure schedule 2 (Table III). Note the change of crack propagation direction and numerous steps in the initiation region. Magnification 3000×.

Morphology of Fracture Surfaces of Reinforced Epoxy Adhesives

Scanning electron micrographs of fracture surfaces of glass-filled epoxy adhesives showed microspheres of various sizes pronounced in clarity and distributed randomly in the epoxy matrix, as shown in Figure 10. Fracture occurs around the spheres as witnessed by the appearance of either intact spheres em-

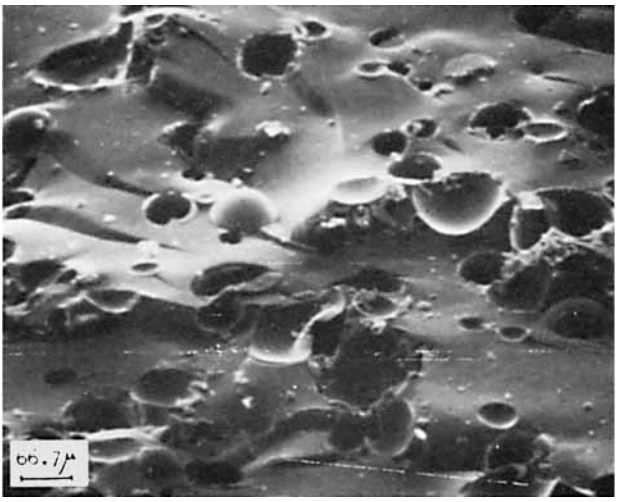

Fig. 10. Scanning electron micrograph of a fracture surface of an aluminum–glass microsphere reinforced epoxy adhesive system subjected to cure schedule 5 (Table III). Tilt angle, 40°; adhesive thickness, 80 μm; magnification 150×.

bedded in the matrix or corresponding holes. Microscopic evidence of the crack migration across the adhesive layer (schematically depicted in Fig. 3) is shown in Figure 11. The crack initiation region contains steps (ridges) also seen on fracture surfaces of pure adhesive joints and bulk specimens.[19]

No replicas of fracture surfaces of C-fiber reinforced epoxies were obtained, owing to surface roughness. Albeit a few replicas of fracture surfaces of glass-filled epoxy adhesives were made; no conclusive results were obtained. Nevertheless, fracture surfaces of various filled thermosets are being investigated presently in our laboratories.

DISCUSSION

In all tested systems, a cohesive failure in the adhesive layer was observed. This is indeed of great importance since the adhesive–adherend interface is eliminated from failure considerations. Thus, it is the adhesive per se that determines the fracture properties of each joint, i.e., critical fracture energies for crack initiation and crack arrest represent the limit of *the adhesive* under given environmental conditions.

All fracture mechanics data are expressed in terms of the critical strain energy release rate ($\mathcal{G}_{Ic}$). Although the critical strain energy release rate is referred to as a material property in this study, it is necessary to realize its dependence upon the loading rate,[18] temperature,[7,24] and aggressive environments such as water or various solvents.[10,16]

In the case of adhesive joints, an additional restriction exists when defining the critical strain energy release rate as a material property. Under otherwise identical testing conditions, varying adhesive thickness can impart a significant effect onto critical strain energy release rate values. For all adhesive joints, a minimum adhesive thickness should be determined beyond which the critical strain energy release rate remains thickness independent. It follows from our results that the bonding thickness constraint on $\mathcal{G}_{Ic}$ as a material property drops above the adhesive thickness of approximately 400 μm. The $\mathcal{G}_{Ic}$ dependence

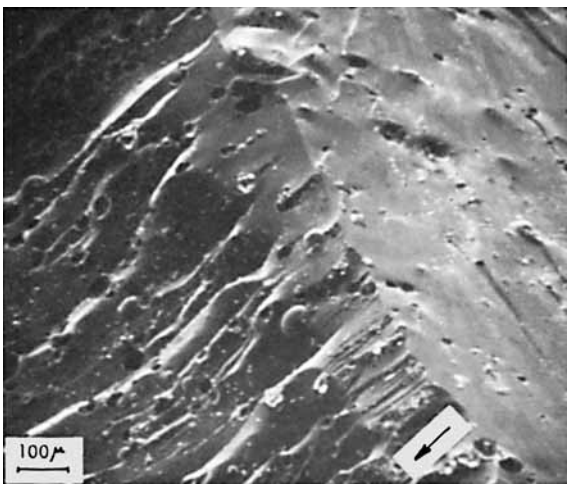

Fig. 11. Same as Figure 10. Tilt angle, 60°; adhesive thickness, 80 μm; magnification 100×. Note the abrupt change of crack propagation direction upon reinitiation.

on the adhesive thickness has also been observed by other workers.[12,24] The difference, however, lies in the shape of the preasymptotic region in which the adhesive thickness directly influences the value of $\mathcal{G}_{Ic}$. Bell-shaped curves, passing through maximum $\mathcal{G}_{Ic}$ at certain bondline thickness, were reported elsewhere; a steadily rising $\mathcal{G}_{Ic}$, eventually reaching an asymptotic value, was observed in this work. Nonetheless, the exact effect and nature of imposed stress conditions at the crack tip in very thin adhesive layers is not quite clear.

In Figure 12, $\mathcal{G}_{Ici}$ and $\mathcal{G}_{Ica}$ values for pure epoxy resin and the C-fiber reinforced formulations are shown for comparison. All specimens had a comparable adhesive thickness and therefore it was excluded as a variable directly determining the magnitude of $\mathcal{G}_{Ic}$. It appears from the results that a significant adsorption of curing agent onto C-fibers takes place at room temperature. This phenomenon explains a required excess of curing agent needed to approximate the curing kinetics of pure epoxy adhesive. It is likely that a preferential adsorption of curing agent onto available C-fiber surface takes place upon mixing. At a certain point, however, C-fiber surfaces become saturated with curing agent and its further addition initiates curing reactions. A synergistic effect of an increase in temperature and a desorption of curing agent from C-fiber surfaces could possibly account for fast occurring curing reactions in lower curing agent concentration systems at higher temperatures (formulation 4, Table III). Apart from the adsorption–desorption role, it appears that the C-fibers, at least at the concentration used in this study (5 phr), do not impart a significant effect on the adhesive fracture properties.

Formulation 4, as shown in Figure 12, has a slightly lower $\mathcal{G}_{Ic}$ value than the pure resin (formulation 1), owing in part to the lack of adhesion between the C-fibers and the epoxy matrix. Higher $\mathcal{G}_{Ic}$ values obtained with formulation

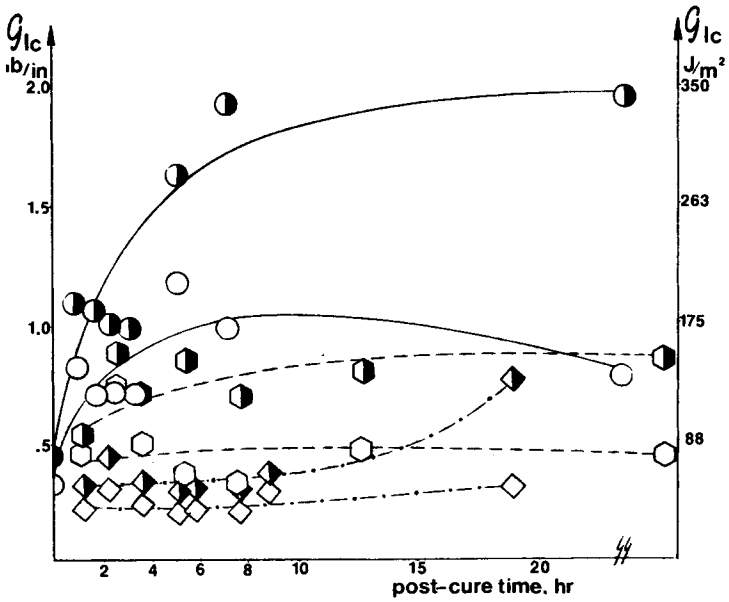

Fig. 12. Comparison of critical strain energy release rate values as a function of postcure time for various adhesive systems (formulations 1 [—, $\mathcal{G}_{Ici}$ (◑), $\mathcal{G}_{Ica}$ (○)]; 3 [---, $\mathcal{G}_{Ici}$ (◑), $\mathcal{G}_{Ica}$ (○)], and 4 [-·-, $\mathcal{G}_{Ici}$ (◆), $\mathcal{G}_{Ica}$ (◇)], Table III).

3 deserve more attention. Careful examination of the critical strain energy release rate dependence on postcure shows that $\mathcal{G}_{Ica}$ values are somewhat comparable to those of pure resin; it is the $\mathcal{G}_{Ici}$ that is significantly higher, giving rise to a higher $\Delta\mathcal{G}_{Ic}$ value. With very high curing agent concentration (25 phr is considerably above the stoichiometric 11 phr), the unreacted curing agent will probably cause a plasticization effect. A direct consequence of this effect would be the blunting of crack tip. This would further involve an increased contribution of inelastic processes which inevitably give rise to higher $\mathcal{G}_{Ic}$ and $\Delta\mathcal{G}_{Ic}$ values. Actually, $\Delta\mathcal{G}_{Ic}$ should be thought of as an indicator of *when* that ultimate brittleness is achieved. A similar consideration of the significance of $\Delta\mathcal{G}_{Ic}$ in bulk systems is discussed elsewhere.[19]

In Figure 13, the effect of various bondline thickness on the fracture properties of a pure epoxy formulation and a glass microsphere reinforced epoxy formulation was compared. Somewhat lower $\mathcal{G}_{Ic}$ values for the filled system are accounted for by the absence of adhesion at the glass sphere–epoxy matrix interface (see Results, Microscopy, second subsection).

Albeit some controversy about the idea of inhomogeneities in brittle thermosets still exists, it appears certain that nodules are an intrinsic characteristic of cured thermosets, representing the sites of higher crosslink density. The size and distribution of nodules on fracture surfaces of pure epoxy adhesives did not change with postcure time, and therefore it is speculated that changes in $\mathcal{G}_{Ic}$ were caused by the additional crosslinking reactions in the internodular matrix. Although reactive groups are less abundant in the internodular matrix, their local mobility is increased at higher postcure temperatures, leading to additional crosslinking reactions. In the vicinity of each step (ridge) in the crack initiation zone, a small region is defined in which the nodules are being diverted towards the step edge. No TEM evidence for deformation of nodules within that region was observed.[19] Therefore, it is suggested that the "flow" of surrounding matrix

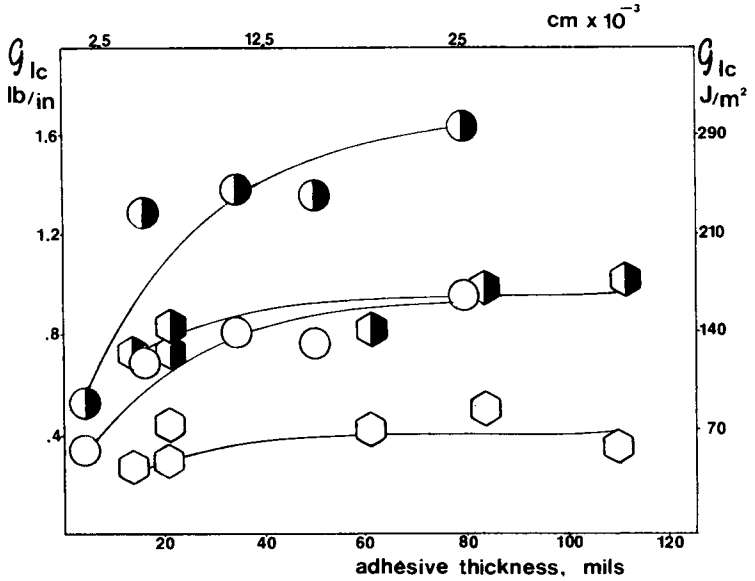

Fig. 13. Comparison of critical strain energy release rate values as a function of adhesive thickness for two adhesive systems (formulations 2 [$\mathcal{G}_{Ici}$ (◑), $\mathcal{G}_{Ica}$ (○)] and 5 [$\mathcal{G}_{Ici}$ (◑), $\mathcal{G}_{Ica}$ (○)], Table III).

that "carries" the nodules characterizes deformation in the crack initiation zone. This is another indication of the higher crosslink density of nodules in comparison with the internodular matrix.

Unfortunately, a solid microscopic evidence of possible changes in nodular size and distribution in the vicinity of reinforcing particles was not obtained. A variation in morphology *within* the same specimen is of considerable importance. If these variations in resin morphology could be unambiguously detected within a specimen, then different parts of the same specimen would be characterized by different mechanical properties. This effect would have a pronounced significance in composite materials. Since the major stress concentration areas in composite materials occur at the matrix–reinforcement interface, resin morphology near the interface becomes instrumental in determining the ultimate mechanical properties and durability of composites. The existence of morphological gradients (variation in size of a morphological unit) in the proximity of reinforcing particles in composite materials has been reported at very few places.[28–30] Moreover, the available information is purely qualitative and an in-depth TEM investigation of this effect is needed. It is instructive to utter the importance of this effect, since because of variations in morphology an assumption that the ultimate mechanical properties of an unreinforced thermosetting resin could be used to predict the behavior of the same resin used as the matrix in a composite material would lead to erroneous results. This problem is presently being investigated in our laboratories.

CONCLUSION

Fracture surfaces of cured nonreinforced epoxy adhesives are shown to be characterized by nodular morphology. Much of the data is consistent with the model of higher crosslink density nodules immersed in a lower crosslink density matrix. The observed changes in fracture energy with postcure time are ascribed to the additional crosslinking reactions in the matrix. Furthermore, fracture energy of investigated epoxy adhesives was found to increase as a function of bondline thickness before reaching an asymptotic value. Regions of crack initiation and crack arrest on all fracture surfaces were characterized by plastic flow. Since the results of this study parallel those of bulk systems,[19] it is suggested that a careful control of cure chemistry can produce desired morphology, which in turn directly influences the ultimate mechanical properties of a resin. Thus, the optimization of mechanical properties of epoxy adhesives could possibly be achieved through a fundamental morphological control. However, to achieve that with reinforced resins, an understanding of morphological gradients is needed first.

Acknowledgment is made to the donors of the Petroleum Research Fund, administered by the American Chemical Society, for partial support of this research. Also, partial funding of this work by the Weyerhaueser Company and the U.S. Forest Products Laboratory is gratefully acknowledged. Special thanks are addressed to Dr. J. A. Koutsky of the University of Wisconsin–Madison and Dr. Dejan Zečević of the University of Belgrade, Yugoslavia, for helpful discussions.

References

1. G. R. Irwin, *Handbuch der Physik,* Vol. VI, Springer, Berlin, 1958, p. 551.
2. E. J. Ripling, S. Mostovoy, and H. T. Corten, *J. Adhes.,* **3,** 107 (1971).
3. G. C. Sih and F. Erdogan, in *Linear Fracture Mechanics,* G. C. Sih, R. P. Wei, and F. Erdogan, Eds., Envo, Lehigh Valley, PA, 1975.
4. E. J. Ripling, S. Mostovoy, and R. L. Patrick, *Mater. Res. Stand.,* **64,** 129 (1964).
5. L. J. Broutman and F. J. McGarry, *J. Appl. Polym. Sci.,* **9,** 609 (1965).
6. J. W. Obreimoff, *Proc. R. Soc. London Ser. A,* **127,** 290 (1930).
7. S. Mostovoy and E. J. Ripling, *J. Appl. Polym. Sci.,* **10,** 1351 (1966).
8. S. Mostovoy, P. B. Crosley, and E. J. Ripling, *J. Mater.,* **2**(3), 661 (1967).
9. G. R. Irwin, in *Treatise on Adhesion and Adhesives,* R. L. Patrick, Ed., Vol. 1, Marcel Dekker, New York, 1967, p. 223.
10. S. Mostovoy and E. J. Ripling, *J. Appl. Polym. Sci.,* **15,** 641 (1971).
11. W. D. Bascom, R. L. Cottington, R. L. Jones, and P. Peyser, paper presented at the American Chemical Society Meeting, Atlantic City, NJ, September 1974.
12. W. D. Bascom, R. L. Cottington, R. L. Jones, and P. Peyser, *J. Appl. Polym. Sci.,* **19,** 2545 (1975).
13. R. A. Gledhill and A. J. Kinloch, *J. Mater. Sci.,* **10,** 1263 (1975).
14. W. D. Bascom, C. O. Timmons, and R. L. Jones, *J. Mater. Sci.,* **10,** 1037 (1975).
15. W. D. Bascom and R. L. Cottington, *J. Adhes.,* **7,** 333 (1976).
16. S. Mostovoy and E. J. Ripling, in *Adhesion Science and Technology,* Vol. 9B, L. H. Lee, Ed., Plenum, New York, 1976.
17. A. J. Kinloch, W. A. Dukes, and R. A. Gledhill, American Chemical Society Meeting Preprint, Philadelphia, April 1975.
18. R. A. Gledhill, A. J. Kinloch, S. Yamini, and R. J. Young, *Polymer,* **19**(5), 574 (1978).
19. J. Mijović and J. A. Koutsky, *Polymer* **20**(9), 1095 (1979).
20. A. W. Bethune, *SAMPE J.,* **3,** 4 (1975).
21. J. Mijović and J. A. Koutsky, *J. Appl. Polym. Sci.,* **23**(4), 1037 (1979).
22. J. Mijović, Ph.D. thesis, University of Wisconsin–Madison, 1978.
23. R. L. Patrick, in *Treatise on Adhesion and Adhesives,* R. L. Patrick, Ed., Vol. 3, Marcel Dekker, New York, 1973.
24. W. D. Bascom, R. L. Cottington, and C. O. Timmons, *J. Appl. Polym. Sci. Appl. Polym. Symp.,* **32,** 165 (1977).
25. J. P. Berry in *Fracture Processes in Polymeric Solids,* B. Rosen, Ed., Wiley, New York, 1964, pp. 157–193.
26. A. S. Tetelman and A. J. McEvily, Jr., *Fracture of Structural Materials,* Wiley, New York, 1967, pp. 287–343.
27. R. A. Gledhill and A. J. Kinloch, paper presented at the International Conference on Fracture Mechanics Techniques, Hong Kong University, March 1977.
28. R. E. Cuthrell, *J. Appl. Polym. Sci.,* **12,** 955 (1968).
29. J. L. Kardos, *Trans. N.Y. Acad. Sci. II,* **35**(2), 136 (1973).
30. J. L. Racich, Ph.D. thesis, University of Wisconsin–Madison, 1977.

Received July 26, 1979
Revised October 17, 1979